Structural phase of femtosecond-laser-melted graphite

T. Dallas and M. Holtz
Department of Physics, Texas Tech University, Lubbock, Texas 79409

H. Ahn and M. C. Downer
Department of Physics, The University of Texas at Austin, Austin, Texas 78712
(Received 28 June 1993; revised manuscript received 16 September 1993)

We have used Raman scattering to investigate the effects of intense laser pulses on the structure of resolidified graphite. Graphite was irradiated with 0.325–3.25-J/cm^2, 620-nm, 90-fs single-laser pulses causing it to melt and rapidly resolidify. Raman studies of the resolidified carbon in the crater show that the rapid annealing process (by pulses with energy fluences ≥ 0.82 J/cm^2) causes a breakdown in the ordered layers of hexagonal carbon rings and disorder in the intraplanar spacing upon resolidification into a nanocrystalline material. The thickness of the nanocrystalline-graphite near-surface layer increases with increasing fluence. Residual planar structure of the resulting material is observed for the various pulse-energy values by comparing the narrow graphitic 1581-cm^{-1} and the broad 1360-cm^{-1} and 1600-cm^{-1} vibrational bands. The interplanar structure of our nanocrystalline graphite is also studied quantitatively via the low-frequency shear mode at 42 cm^{-1}. The Raman spectrum of our glassy carbon is found to be well described by planar ordering approximately 2 to 3 layers in extent using a simple correlation function approach. Our results indicate a layered morphology is present in our nanocrystalline graphite, confirming a strong sp^2 bonding character.

I. INTRODUCTION

Much work has been done on the properties of liquid carbon immediately after annealing by a short, highly intense laser pulse.[1–4] State-of-the-art laser systems allow femtosecond pulses with sufficient intensity to melt various solids. In highly ordered pyrolytic graphite (HOPG, which we will refer to simply as graphite), photons are absorbed by electronic interband transitions within the first several hundred Å of the irradiated surface ($d_{\rm OPT}=1/\alpha=300$ Å) in graphite at $\lambda=620$ nm.[1] This large and rapid energy transfer causes the electrons to reach a highly excited state, efficiently breaking all bonds and thereby melting the solid. Through collisions, the electrons rapidly transfer kinetic energy to the carbon ions which, conceptually, produce a small puddle of highly energetic molten carbon on a very short time scale.

Reitze, Ahn, and Downer[1] used reflectance measurements immediately following the laser anneal pulse to observe a sharp increase in the reflectance of the melted graphite. This, along with carbon release from the surface, has been interpreted as evidence that the graphite has reached a liquid phase. Steinbeck *et al.*,[2] Braunstein *et al.*,[3] and Elman *et al.*[4] have done postmortem studies on laser-damaged graphite, similar to our present work. Their results show the formation of randomly oriented graphite platelets which vary in size depending on the laser anneal energy. The nanosecond and picosecond duration laser pulses used in Refs. 2–4 are, however, much longer than the femtosecond pulses used here, and could potentially lead to different resolidification phenomena.

This study will confirm that the graphite was indeed melted and will attempt to reconstruct physical effects based on the Raman signature of the resolidified carbon atoms. Because the vibrational spectrum is an accepted signature of individual solid phases, Raman spectroscopy is well suited to the task of accurately determining the phase or phases of the material present. Furthermore, the small (≈ 10 μm) diameter and shallow depth of the Raman probe make this technique perfect for studying the small sample volumes produced in the melting experiment.

The Raman spectrum of graphite is characterized by two zone-center optic phonons, both of which propagate along the crystalline c axis. Figure 1 depicts the normal mode displacements of these two phonons. One high-energy phonon (E^2_{2g}) corresponds to in-plane, covalent carbon-carbon bond stretching and exhibits a narrow Raman band at 1581 cm^{-1}. The low-energy phonon (E^1_{2g}) was first measured by Nemanich and Solin,[5] and corresponds to a shearing motion of the weak, interplanar van der Waals bonds. It has a vibrational energy of 42 cm^{-1} and exhibits a very weak scattering intensity.

In amorphous (and significantly disordered) materials, however, Raman scattering by vibrations throughout the entire vibrational spectrum is allowed.[7] This leads to Raman spectra in amorphous materials which mimic the vibrational density of states. This is in stark contrast to the restrictive $\mathbf{k}=0$ constraint imposed on Raman scattering in crystalline materials. The high-frequency vibrational spectrum of so-called glassy carbon has two broad bands centered near 1600 and 1360 cm^{-1} due to finite crystallite size effects.[6] The former band corresponds to vibrations of the nanocrystalline material with parent vibrations similar to the 1581-cm^{-1} mode in graphite. The broad 1360-cm^{-1} band is accepted as being due to disorder-induced Raman activation of zone-boundary phonons in

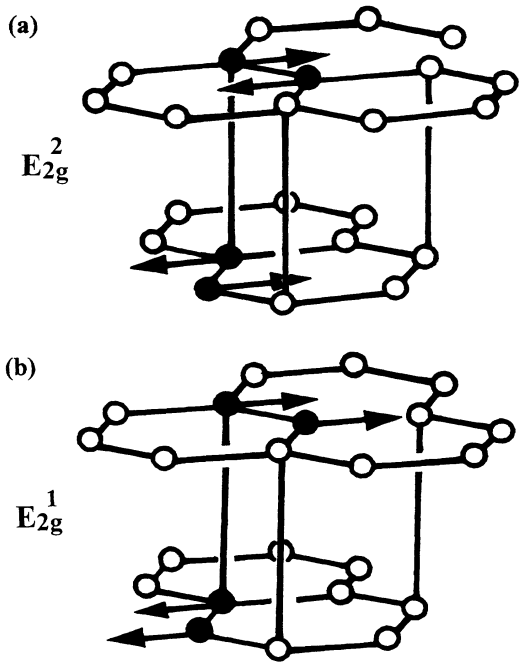

FIG. 1. Zone-center vibrational modes in graphite. The high-energy phonon (E_{2g}^2) corresponds to in-plane, covalent carbon-carbon bond stretching and exhibits a clear Raman band at 1581 cm^{-1}. The low-energy phonon (E_{2g}^1) at 42 cm^{-1} corresponds to a shearing motion of the weak, interplanar van der Waals bonds.

crystalline graphite.[8]

In this paper, we present Raman-based studies which improve the current picture of glassy carbon and its relationship to graphite. By achieving a quantitative understanding of the low-frequency Raman spectrum of the laser pulse produced glassy carbon, a detailed understanding of the *interplanar* structure is reached. We find that our material consists of graphite nanocrystallites of typical in-plane dimension $L_a \approx 60$ Å and out-of-plane dimension $L_c \approx 8.5$ Å. For this reason, we shall proceed to name our disordered material nanocrystalline graphite (*n*-graphite). From our results, a phenomenological picture of the resolidification of graphite is developed, subsequent to laser-pulse melting. The remainder of this paper is organized as follows. After a brief description of the experimental procedures, we discuss our postmortem Raman measurements of laser irradiated graphite in the high vibrational-energy regime. Following these results, we exhibit Raman evidence for weak interplanar ordering in *n*-graphite produced using this method. We then summarize our findings.

II. EXPERIMENTAL PROCEDURE

The sample studied was HOPG graphite which had been irradiated with laser pulses 90 fs in duration at a wavelength of 620 nm. Pulses were produced using a colliding pulse mode-locked (CPM) ring dye laser followed by a four-stage Nd:YAG pumped optical dye amplifier system operating at a 10-Hz repetition rate. The pulse intensities were varied over a range to produce energy densities (fluences) greater than the threshold melt energy density.[1] These pulses caused carbon atoms to be liberated from the surface producing a small crater. Craters were elliptical in shape with a major axis ~ 50 μm across. A detailed description of the laser melting process is given in Ref. 1.

Raman scattering was generated using a continuous argon-ion laser running at the 514.5-nm green line. The backscattered light was dispersed through a 0.5-m monochromator which passed the light to a charge coupled device (CCD) 512×512 multichannel analyzer. Using this, we were able to simultaneously measure a spectral range spanning 600 cm^{-1}, with a resolution of approximately 1 cm^{-1}. Emission from a low-pressure neon lamp was used to calibrate the CCD. In order to see the 50-μm-diam craters, a TV camera was connected to a microscope. The Raman laser probe spot was one-fifth the size of the crater, making it possible to precisely focus the laser on the center of each crater. All measurements in the high-energy regime were done in air at room temperature.

In order to measure the low-energy, 42-cm^{-1} interplanar shearing vibration, we used a krypton-ion laser running at the 647.1-nm resonance enhancing line.[5] Focusing and positioning of the laser spot was once again accomplished using a microscope. Scattered light was collected and prefiltered by a 0.5-m single grating monochromator. The surviving narrow wavelength range of light was then analyzed by a 0.85-m double monochromator producing a triple-additive-dispersive Raman system. The spectrometers were stepped synchronously in wavelength via computer control. A photomultiplier was used in the photon-counting mode to detect the analyzed photons. This triple system is very effective in excluding extraneous parasitic scattering of the laser line and allows the observation of very low-energy vibrations.[9] The graphite sample was kept under an argon atmosphere to reduce the observed intensity of the known Raman spectrum of air. All experiments were done at room temperature.

III. RESOLIDIFIED STRUCTURAL PHASE OF LASER-PULSE ANNEALED GRAPHITE

Figure 2 compares the Raman spectra from graphite with that taken from the center of the crater formed with a laser irradiation energy density of 0.82 J/cm^2. The virgin material shows the characteristic sharp graphite peak at 1581 cm^{-1} [full width at half maximum (FWHM) = 15 cm^{-1}]. Below 0.82 J/cm^2, there is no evidence of disorder, indicating a return to the normal graphite structure upon resolidification. This is consistent with the work of Braunstein *et al.*[3] which was done with pulses of longer duration but comparable energy densities. The lowest-energy density above threshold shown in Fig. 2, 0.82 J/cm^2, shows a superposition of a sharp 16-cm^{-1}-wide graphite peak at 1581 cm^{-1} on top of a broadband which is centered at 1600±10 cm^{-1}. The broad Raman signal underlying the graphite 1581-cm^{-1} line indicates a disordered phase of carbon has been formed which is consistent with what is commonly called glassy carbon, but

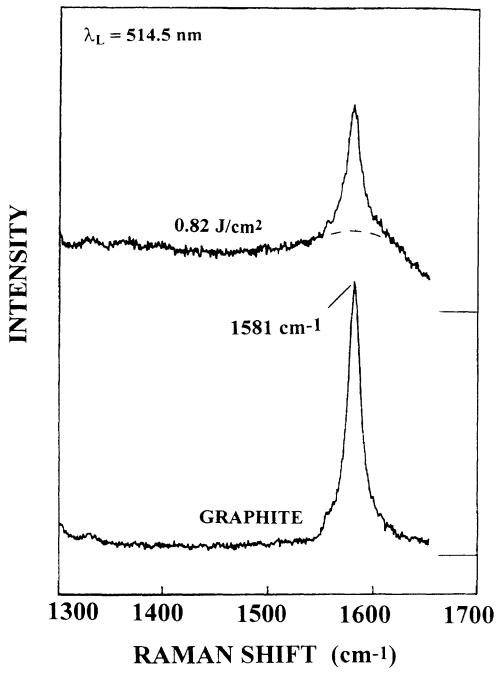

FIG. 2. Room-temperature Raman spectra of the graphite starting material and of the 0.82-J/cm^2 laser irradiated material. The latter spectrum shows a superposition of the graphite peak at 1581 cm^{-1} on top of a broadband centered at 1600±10 cm^{-1}. The horizontal lines at the right-hand border indicate baselines for the 0.82-J/cm^2 spectrum.

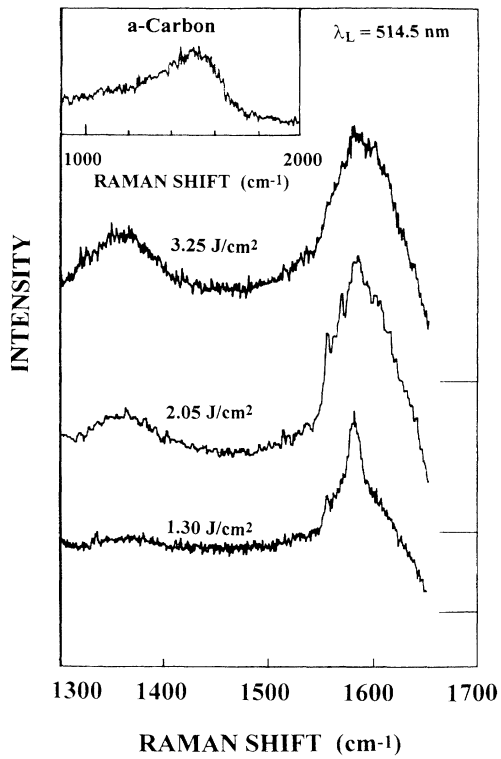

FIG. 3. At an energy density of 1.30 J/cm^2, a broad feature begins to form at 1360 cm^{-1} while the broadband at 1600 cm^{-1} continues to grow with a weak 1581-cm^{-1} graphite band superimposed. The 2.05- and 3.25-J/cm^2 spectra show no sign of undamaged graphite as the depth of *n*-graphite grows beyond the probe depth of the laser. The inset shows the Raman spectrum of graphitic amorphous carbon. The horizontal lines at the right-hand border indicate baselines for each spectrum.

in the present context is better described as *n*-graphite. As the long-range order of the graphite breaks down, **k** is no longer a valid quantum number and we see Raman scattering from vibrations present in the nanocrystalline medium which do not correspond to the **k**=0 optic phonons observed in graphite crystals. This spectrum indicates that the laser is probing both the damaged near-surface regime and the underlying graphite.

Spectra from higher irradiation fluences are presented in Fig. 3, supporting our conclusion of an *n*-graphite surface. The 1.30-J/cm^2 spectrum shows a reduction in intensity of the graphite peak as the disorder region grows,[3] and becomes substantially deeper than the optical penetration depth of our laser light. The band from the underlying graphite (1.30 J/cm^2) is superimposed on a broadband centered at 1600 cm^{-1} (FWHM=80 cm^{-1}), identical to the 0.82 J/cm^2 irradiated graphite. Also, by an energy density of 1.30 J/cm^2, a broad feature is seen at 1360 cm^{-1}. The 2.05- and 3.25-J/cm^2 spectra in Fig. 3 show no hint of undamaged graphite, indicating that we probe only the near-surface *n*-graphite with 514.5-nm Raman excitation.

The spectra corresponding to the near-surface damaged material are in good agreement with measurements of ion-damaged glassy carbon.[10,11] The ion-damaged material in Ref. 10 and 11 gradually transforms from glassy carbon into amorphous carbon (as in the inset to our Fig. 3) with sufficient ion dose. We find that our spectra best agree with their glassy carbon following 320-keV Xe^+ implantation to a total fluence dose of 9×10^{13} ions/cm^2. The similarity between glassy carbon damaged in this manner and our results supports the identification of our material as nanocrystalline graphite, consisting of small platelets of graphite smaller in dimension than glassy carbon. Also present in our spectra, and in those of Refs. 10 and 11, is a broad underlying background spectrum. The exact origin of this background is not known, and the spectral range of our data does not permit adequate deconvolution to determine its nature.

An estimate of the thickness may now be generated based on the observed onset of *n*-graphite formation. From our results, this level ranges between 0.52 and 0.82 J/cm^2 (the former fluence is the first step measured below the latter). Since we measured no energy densities between these two values, we will use the average of these two values as the threshold energy density above which the carbon resolidifies as *n*-graphite and below which it recrystallizes as graphite. As a by-product of our measurements, we can estimate the depth at which the laser-pulse peak intensity falls below the value needed to form *n*-graphite (0.67±0.15 J/cm^2), assuming a simple exponential attenuation. Laser-pulse attenuation is assumed to be sufficiently fast that the absorption coefficient can be taken as that of graphite under ambient

conditions. This assumption is found to be consistent with an independent analysis in Eq. (2). For the various laser energy pulse densities used here, we calculate the cutoff depth of the damage threshold (i.e., the depth at which the fluence in the irradiation pulse drops below the value needed to create *n*-graphite) according to

$$I(z)=I_0 e^{-\alpha_G z}, \quad (1)$$

where $1/\alpha_G=300$ Å (Ref. 1) and z is the depth. I_0 represents the laser fluence at the $z=0$ surface. Results for $z=d_{\text{cutoff}}$ where the energy pulse density reaches the damage threshold of 0.67 ± 0.15 J/cm^2 are listed in Table I, along with the estimated thickness of *n*-graphite produced. We do not account for the carbon losses due to evaporation from the surface, which can decrease the thickness of the *n*-graphite layer measured.[1]

We now proceed to test the internal consistency of our thicknesses from Eq. (1) via the measured Raman spectra. The Raman intensity of the underlying graphite peak will be attenuated by the *n*-graphite (nG) overlayer characterized by $1/\alpha_{\text{nG}}\approx 1/\alpha_{\text{GC}}=580$ Å,[12] the optical penetration depth at 514.5 nm, and thickness d_{nG}. The scattering volume in the Raman intensity has a depth (scattering length) term

$$I_G \sim \langle l \rangle \sim e^{-2\alpha_{\text{nG}} d_{\text{nG}}} \int_{d_{\text{nG}}}^{\infty} e^{-2\alpha_G z} dz, \quad (2)$$

which is readily integrated. The factor of 2 in each exponent describes attenuation of the light as it enters the sample and as it exits in the backscattering configuration. By comparing the Raman integrated intensity of the 1581-cm^{-1} band of undamaged graphite ($d_{\text{nG}}=0$) to that of the 0.82-J/cm^2 spectrum, we arrive at a $d_{\text{nG}}\approx 60\pm10$ Å at a wavelength of 514.5 nm. For the 1.30-J/cm^2 energy fluence, where we see a weaker graphite 1581-cm^{-1} peak, we estimate $d_{\text{nG}}\approx 130\pm22$ Å. Most of the error reported comes from the estimated 10% precision of the Raman intensity ratio. Since the graphite-peak intensity following the 1.30-J/cm^2 laser pulse is smaller than for the 0.82-J/cm^2 pulse, the latter generates a better estimate of d_{nG}. Both estimates are within the total error estimate. The agreement between the two different d_{nG} values from Eqs. (1) and (2) is remarkable, making the internal consistency of this analysis satisfying, and supports our interpretation of the graphite Raman signal as being due to underlying graphite material either unmelted or recrystallized after melting. Furthermore, the resulting agreement between d_{nG} obtained using Eqs. (1) and (2) justifies the simple assumption used in Eq. (1) that the femtosecond pulses are absorbed by a material which is described solely by the absorption coefficient of graphite. This is in spite of the fact that the graphite is in the process of melting (by the pulse) and its optical properties are rapidly changing.

TABLE I. The thicknesses of the near-surface *n*-graphite regions obtained from Eqs. (1) and (2). d_{cutoff} values of zero indicate that no glassy carbon was observed for these fluences. No entry in column 3 indicates no glassy carbon or no graphite peak clearly observed.

I_0 (J/cm^2)	$d_{\text{cutoff}}\approx d_{\text{nG}}$ (Å) [Eq. (1)]	d_{nG} (Å) [Eq. (2)]
0.325	0	
0.52	0	
0.82	60±13	60±10
1.30	200±40	130±22
2.05	335±70	
3.25	470±100	

The 1360-cm^{-1} disorder-induced vibrational band, which corresponds in energy to zone boundary vibrations in graphite, continues to grow while the 1600-cm^{-1} broad peak shrinks and broadens with increasing irradiation energy density. This is taken as evidence of slight variance in the microstructure of the *n*-graphite produced by differing pulse energy densities, i.e., differing characteristics of the melt phase. From the range of energy densities studied here, we anticipate that little variation in the resolidified material will be observed with higher densities, but further investigation is required to clarify this point.

Comparisons between the laser-melted graphite and other popular phases of carbon were also made. The inset of Fig. 3 shows the Raman spectrum of an arc evaporated graphitic amorphous carbon film.[13] We find no simple correlation between this spectrum and that of *n*-graphite or glassy carbon,[2,6,7,10,11] outside of the overlap in the overall energy range subtended. This is clear evidence that these carbon phases possess dissimilar microstructures. No evidence of diamond formation is found. Primarily responsible for the lack of diamond formation is the fact that graphite is the thermodynamically preferred state. Since the mass densities of graphite (2.55 g/cm^3) and diamond (3.5 g/cm^3) are considerably different, there is an additional volume-related stumbling block to rapidly converting graphite to diamond. Most of the energy provided by the laser pulse is acquired by the electrons, and is dissipated by the surrounding unmelted graphite. We also found no evidence of fullerene production and retention in the crater.

Our results show that laser pulses of sufficient energy density cause the molten graphite to resolidify into a form of carbon similar to graphite in that intermittent graphite structure, i.e., crystallites, is formed. We envision our nanocrystalline material as containing small graphite microcrystalline regions, presumably interconnected by a volume-filling disordered structure. Tuinstra and Koenig[6] have shown that the intensity ratio of the broad 1600- and 1360-cm^{-1} Raman bands gives a quantitative indication of L_a, the *in-plane* dimension of the graphite crystallites. In the analysis of Braunstein *et al.*,[3] for a much slower melting process, the relatively long-lasting (>ns) heat and pressure generated by their laser pulses cause an annealing mechanism which permits the formation of large graphite crystallites. The finite diameters of the platelets result in a breakdown of the $\mathbf{k}=0$ crystal Raman selection rule, activating scattering by zone-edge phonons near 1360 cm^{-1}. They propose that >100-Å graphite crystal platelets form due to their annealing, which they identify to be similar to glassy carbon. Based on the analysis of Ref. 6, the implied average

graphite crystallite size for each energy fluence case we measured here is ≈ 60 Å. This estimate is based solely on Raman measurements using the 514.5-nm excitation. There may be some variance with estimates generated using other laser wavelengths, but we rely here on the original work of Tuinstra and Koenig,[6] who used 488.0- and 514.5-nm sources. We will return to the validity of this result in Sec. IV.

IV. THE INTERLAYER STRUCTURE OF NANOCRYSTALLINE GRAPHITE

The *n*-graphite interplanar structure is also altered due to the inhomogeneities in planar structure created by the laser-melting and resolidification process. We studied the interplanar structure of our *n*-graphite via the low-energy, 42-cm^{-1} phonon corresponding to the shear mode between graphite planes. This mode should be extremely sensitive to interplanar disorder, and essentially absent if no planar structure exists. The Raman spectrum of the graphite starting material is shown in Fig. 4. Seen is a weak and relatively narrow peak at 42 cm^{-1}, in agreement with previous observations.[5] The 6-cm^{-1} linewidth is primarily due to the $\approx$5-cm^{-1} spectral bandpass of the Raman system. Following the 3.25-J/cm^2 laser pulse (for which the *n*-graphite region is sufficiently thick to ensure that we measure only that material), the peak broadened to 10 cm^{-1} and the maximum intensity position weakly redshifted to 39 cm^{-1}. We take this as evidence that annealing has altered the planar structure, but not entirely destroyed it. The implied warping, puckering, and misalignment propagates through the relatively floppy carbon sheets. The resulting structure is still locally sheetlike, but not strictly planar. Interlayer correlation is therefore only weakly present, in contrast to the well-ordered graphite starting crystals.

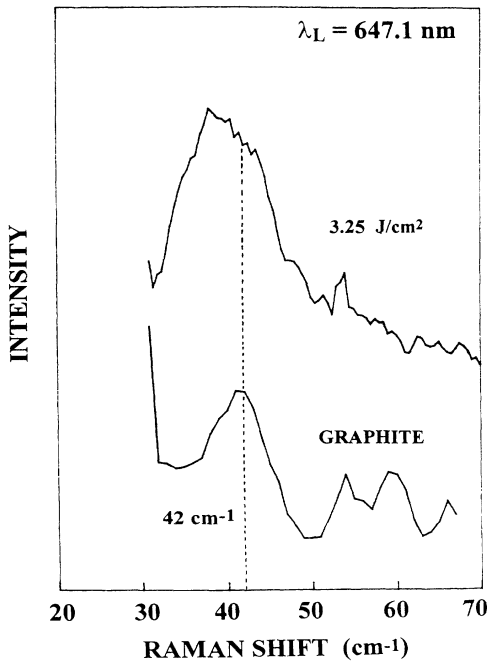

FIG. 4. The interplanar E^1_{2g} [see Fig. 1(b)] shear mode of pure graphite has a vibrational energy of 42 cm^{-1} and exhibits a very weak scattering intensity. The *n*-graphite (following the 3.25-J/cm^2 laser pulse) exhibits a slightly redshifted (to 39 cm^{-1}) and broadened peak indicating a short-range-ordered planar structure (see text).

To describe the loss of interplanar regularity, we develop a model to describe the effect of diminishing long-range order along the *c* axis of graphite. This model uses the vibrational dispersion of graphite for phonons which correspond to interplanar shear motion. This choice of vibrational signature is reasonable, since we believe the *n*-graphite to be closely related to graphite. Since the "planes" in *n*-graphite are not well coordinated, crystalline order quickly vanishes as one moves from one sheet to the next. This type of treatment of the effects of short-range crystalline order on Raman scattering has been successfully used to describe spectra of cubic microcrystalline silicon[14] and implanted GaAs.[15] In that case, the $\mathbf{k}=\mathbf{0}$ selection rule fails due to the finite extent of the crystallites. Failure of the selection rule is manifested in the long-wavelength optic modes being activated due to interference with the crystallite boundaries, while shorter-wavelength (zone-edge) modes are only weakly influenced. A Gaussian function is used to represent a distribution in crystallite size. In our case, we describe selection-rule breakdown only along the *c* axis of the graphite crystal. We express the intensity as a function of energy for the 42-cm^{-1} phonon branch as

$$I(\omega)\sim\int \exp(-q^2L_c^2/4)\frac{dq}{\{[\omega-\omega(q)]^2+[\Gamma/2]^2\}}\ , \qquad (3)$$

where L_c is the interplanar correlation length in the *n*-graphite material and is the only adjustable parameter in our model. Γ is the FWHM linewidth of the Lorentzian parent 42-cm^{-1} mode (6 cm^{-1}, in our case). Integration in Eq. (3) is in one *k*-space dimension since we describe here only the breakdown in coherence in the graphite *c*-axis direction. The dispersion of the optic branch is downward as one moves away from the zero center, and is adequately approximated by

$$\omega(q)=A+B\cos(\pi q)\ , \qquad (4)$$

where $A=36$ cm^{-1} and $B=6$ cm^{-1} are taken from Refs. 16 and 17. By using Eqs. (3) and (4), and varying the interplanar correlation length L_c, we find that a mean correlation length of 2.5 graphite planes best describes the spectrum in Fig. 4. This indicates that long-range interplanar order has been substantially reduced, by the melting-resolidification process, to an average value of 8.5 Å.

These results are consistent with very weak epitaxial growth. Since the melted carbon is sitting on a graphite lattice, it tends to resolidify in a similar lattice. Also, the sp^2 bonding configuration of graphite is the most desirable phase of carbon given the above-noted crystal seeding and volume constraints. As a result, the resolidified material best resembles graphite in structure, possessing a weak interplanar correlation and, possibly, a puckered planar structure. Additionally, defects were induced by

carbon atoms displaced following the laser anneal, causing a disordered structure to form.

V. CONCLUSIONS

Our results show that above a threshold energy of approximately 0.67 J/cm^2, increasing energy densities produce increasingly deeper regions of disordered carbon situated above undamaged graphite. Below this threshold, pulse melted graphite epitaxially recrystallizes. Presumably, the higher intensities drive the liquid carbon farther from equilibrium, permitting a disorder phase to solidify. The Raman spectrum of the surface layer indicates a breakdown of the $\mathbf{k}=0$ optic-phonon selection rule imposed by crystalline order is consistent with the *n*-graphite carbon phase. We find that a weak planar structure persists. Low-frequency Raman spectra in the graphite shear-vibration range provide evidence that *n*-graphite retains some discrete shearing motion. A finite correlation length of approximately 8.5 Å along the *c* axis describes the observed Raman measurements well, and confirms that *n*-graphite has layered character with a very short interlayer correlation length. The presence of a shear mode clearly indicates that *n*-graphite, and likely also glassy carbon, has a strong sp^2 bonding character, although a mixture with sp^3 bonds could be a viable explanation for the disruption of planar order and planar stacking order, and the interconnection between nanocrystallites. Finally, these results show that the crystallinity of graphite has been altered by the high-energy density, ultrashort duration laser pulses, and provide an improved understanding of the morphology of this disordered material.

ACKNOWLEDGMENTS

We would like to thank J. R. Dennison for a thorough reading of this manuscript. The authors at Texas Tech acknowledge support from the Texas Tech Research Enhancement Fund. Work conducted at University of Texas-Austin was supported by the Robert A. Welch Foundation (Grant No. F1038) and by The National Science Foundation (Grant No. DMR8858388). T.D. would like to thank the Bucy Foundation and ARCS for financial support.

[1]D. H. Reitze, H. Ahn, and M. C. Downer, Phys. Rev. B **45**, 2677 (1992).

[2]J. Steinbeck, G. Draunstein, J. Speck, M. S. Dresselhaus, C. Y. Huang, A. M. Malvessi, and N. Bloembergen, in *Beam-Solid Interactions and Transient Processes,* edited by M. O. Thompson, S. T. Picraux, and J. S. Williams, MRS Symposia Proceedings No. 74 (Materials Research Society, Pittsburgh, 1987).

[3]G. Braunstein, J. Steinbeck, M. S. Dresselhaus, G. Dresselhaus, B. S. Elman, T. Venkatesan, B. Wilkens, and D. C. Jacobsen, in *Beam-Solid Interactions and Phase Transformations,* edited by H. Kurz, G. L. Olsen, and J. M. Poate, MRS Symposia Proceedings No. 51 (Materials Research Society, Pittsburgh, 1986).

[4]B. S. Elman, G. Braunstein, M. S. Dresselhaus, and G. Dresselhaus, Phys. Rev. B **29**, 4703 (1984).

[5]R. J. Nemanich and S. A. Solin, Phys. Rev. B **20**, 392 (1979).

[6]F. Tuinstra and J. L. Koening, J. Chem. Phys. **53**, 1126 (1970).

[7]R. Zallen, *The Physics of Amorphous Solids* (Wiley, New York, 1983).

[8]B. S. Elman, M. S. Dresselhaus, G. Dresselhaus, E. W. Maby, and H. Mazurek, Phys. Rev. B **24**, 1027 (1981).

[9]M. Holtz, S. A. Solin, and T. J. Pinnavaia, Phys. Rev. B **48**, 13 312 (1993).

[10]S. Prawer and C. J. Rossouw, J. Appl. Phys. **63**, 4435 (1988).

[11]S. Prawer, F. Ninio, and I. Blanchonette, J. Appl. Phys. **68**, 2361 (1990).

[12]M. W. Williams and E. T. Arakawa, J. Appl. Phys. **43**, 3460 (1972).

[13]J. O. Stoner, J. Appl. Phys. **40**, 707 (1969).

[14]H. Richter, Z. P. Wang, and L. Ley, Solid State Commun. **39**, 625 (1981).

[15]K. K. Tiong, P. M. Amirtharaj, F. H. Pollak, and D. E. Aspnes, Appl. Phys. Lett. **44**, 122 (1984).

[16]R. Al-Jishi and G. Dresselhaus, Phys. Rev. B **26**, 5414 (1981).

[17]S. A. Solin, Physica B **99**, 443 (1980).